Sensors and Materials, Vol. 38, No. 4 (2026) 2129–2147
MYU Tokyo

S & M 4427

Design of Gravity Casting Parameters for Bearing Seat in Wind Turbine by Multi-objective Optimization Approach

Jian Wei,[1,2] Chi-Hsin Yang,[1*] and Hai-Lian Hong[1,3]

[1]School of Mechanical and Electric Engineering,
Sanming University, Sanming 365004, Fujian Province, China
[2]Fujian University Engineering Research Center of Modern Mechanical Design and Manufacturing Technology,
Sanming 365004, Fujian Province, China
[3]School of Navigation, Xiamen Ocean Vocational College, Xiamen 361012, China

(Received November 18, 2025; accepted April 22, 2026)

Keywords: gravity casting, bearing seat, Box–Behnken design (BBD), response surface methodology (RSM), analysis of variance (ANOVA)

The process parameters for gravity casting bearing seats in wind turbines are optimized using a multi-objective optimization framework that combines casting process numerical simulation, response surface methodology (RSM), the dragonfly optimization algorithm (DOA), and the X-ray detection of casting product quality. The experiments follow a Box–Behnken design (BBD) to evaluate key casting parameters and response indicators. The crucial variables included are pouring speed, pouring temperature, and mold temperature. Defect volume fraction (*DVF*) and secondary dendritic spacing serve as response markers. Regression analysis develops nonlinear input–output models, whereas the analysis of variance assesses model significance. DOA expands the population to identify optimal casting parameters, with numerical simulations confirming the best option. Results demonstrated the optimized parameter set of mathematical models. That is, the mold temperature is 100 °C, the pouring speed is 0.07 m/s, and the optimal pouring temperature is 1380 °C. These casting parameters were used to fabricate the bearing seat experimentally, and defects in the products were detected using sensors. Metallographic observation by X-ray detection confirmed that the bearing seat exhibited strong mechanical properties without any flaws detected by X-ray. The proposed framework faces limitations and pending problems including nonuniform casting quality owing to optimized parameters from simplified models and time-consuming, costly experimental validation. Overcoming these challenges is central to our subsequent work.

1. Introduction

Wind turbines convert wind energy into electricity for the national power grid, serving residential, industrial, and commercial needs. This technology is favored for its environmental sustainability, low operating costs, modular design, efficient land use, and rapid

*Corresponding author: e-mail: 20190207@fjsmu.edu.cn
https://doi.org/10.18494/SAM6057

ISSN 0914-4935

advancements.[1] Key components such as blades, hubs, and main shafts are typically made from ductile iron and alloy steel through precision casting and forging methods.[2–4]

Gravity casting is a conventional process that fills molds with molten metal using gravity without external pressure required. It is widely used for nonferrous alloys, such as aluminum and copper-based ones, owing to its stable, laminar filling, which minimizes turbulence and porosity. The process supports both permanent metal and expendable sand molds, offering flexibility for low-to-medium volume production and varied part geometries. The bearing seat of the hub is usually produced via gravity casting. While this method can lead to defects such as pores and shrinkage cavities, and requires additional machining owing to surface roughness, its cost-effectiveness makes it popular in onshore wind power applications.[5–7]

In Refs. 8 to 10, the researchers utilized the Taguchi experimental design method by selecting key process parameters, such as pouring temperature, pouring speed, and mold temperature, to improve casting quality by enhancing tensile strength and hardness while minimizing porosity. In Refs. 11 and 12, the Taguchi method was integrated with gray relation analysis to optimize key gravity casting parameters, including pouring temperature and mold preheating, for demonstrating particular effectiveness by multi-objective optimization. These studies also examined the factors affecting shrinkage porosity, including cooling rate and carbon equivalent, through experiments and simulations.

Recent research has emphasized advanced optimization algorithms and experimental techniques to enhance cast component quality via adjustments in gravity casting parameters. In Ref. 13, a new neural network model that combines quantitative learning vectors with the back propagation algorithm to capture nonlinear relationships between process parameters and performance metrics in low-pressure die-casting (LPDC) was developed. An optimization method integrating artificial neural networks with genetic algorithms (GAs) was introduced to improve LPDC settings significantly for aluminum alloy carburetor shells. In Ref. 14, GA was paired with fuzzy logic methods to analyze the relationship between process parameters and defect formation; the analysis of variance (ANOVA) identified key influential parameters, providing data-driven insights for process optimization. Deng *et al.*[15] proposed a novel algorithm for comprehensive parameter optimization in updated die-casting processes, demonstrating real-world effectiveness while introducing innovative strategies for designing casting parameters that support future advancements in die-casting technology.

Owing to rapid advances in computer-aided engineering within the casting industry, design engineers can now accurately simulate casting processes using numerical techniques. Researchers have developed finite element models to replicate these processes, predict part quality and defect patterns, and enable quantitative quality assessments.[16–24] These advancements have significantly improved casting quality evaluation by transitioning from traditional qualitative methods to precise quantitative techniques for reliable defect analysis.

Zheng *et al.*[23] investigated the solidification behavior of aluminum alloy wheels in LPDC. They utilized numerical simulation to assess how microstructures and defects affect wheel performance, evaluating changes in temperature, velocity, solid phase fraction, and defect distribution. This led to a creative process design approach that significantly reduced shrinkage and defect formation, offering practical guidance for enhancing aluminum wheel manufacturing.

Li *et al.*[16] developed a simulation method using response surface methodology (RSM) to predict minimized casting defects and identify the corresponding optimal process parameters. A regression-based mathematical model was first validated through 17 simulations based on the Box–Behnken design (BBD) and analyzed with ANOVA. Furthermore, an experimental trial production was conducted, and radiographic inspection by X-ray detection revealed no casting defects. He *et al.*[24] systematically optimized LPDC parameters for large aluminum alloy wheel hubs using casting simulation, RSM, and GA. On the basis of BBD, key variables, namely, pouring temperature, mold temperature, and holding pressure, were selected to establish nonlinear relationships between inputs and outputs such as defect volume fraction (*DVF*) and secondary dendrite arm spacing (*SDAS*). A regression-based model was employed to evaluate performance indicators and, when integrated with GA, effectively identified the optimal casting parameters. In addition, hub experimental samples passed X-ray inspection, and the results indicated that the corresponding optimal casting process parameters yielded defect-free castings.

Previous studies[16–24] often overlook the complex interactions among these casting parameters, highlighting the need for more systematic optimization efforts. Furthermore, experimental validation via physical casting trials remains essential to confirm its efficacy. The optimization of process parameters and solidification control techniques for ductile iron gravity casting is still underdeveloped. On the basis of a review of current research and methods in casting technologies, in this study, we outline its research motivation.

In gravity casting, molten metal fills the mold cavity solely under Earth's gravity. Unlike squeeze casting, which is applied pressure to enhance melt flow, gravity casting inherently suffers from limited melt mobility. To ensure the structural reliability of casting products, comprehensive defect evaluation techniques are essential, such as X-ray radiography and metallography. In this study, we focused on the ductile iron bearing seat in gravity casting to provide valuable theoretical and experimental insights.

The novelty of this study is the introduction of a multi-objective optimization framework, combined with RSM, the dragonfly optimization algorithm (DOA), and the casting product quality by X-ray detection, for gravity casting process parameter design. The main contributions of this study are summarized as follows.

(1) The ProCAST simulation software is utilized to create a finite element model for the gravity casting of the bearing seat. Numerical simulations are performed, and the temperature field is validated and adjusted with experimental data to ensure accuracy.
(2) A gravity casting experiment is designed using BBD, with each setup modeled through simulation tools.
(3) A prediction model for casting quality is developed by correlating response results with experimental parameters, and its reliability is evaluated using ANOVA.
(4) Process parameters are optimized via RSM and DOA.[25] Multi-objective optimization identifies optimal parameters, followed by minor adjustments to enhance continuous solidification and improve casting quality in the laboratory.
(5) With the optimized casting parameters determined in Step (4), an experimental casting is produced and subsequently inspected via X-ray radiography to assess product quality. Moreover, the validation of the proposed multi-objective optimization framework for gravity casting is evaluated.

The proposed framework has several limitations and pending problems requiring thorough evaluation. First, it relies on simplified models, such as numerical simulations and empirical selected key factors, which cannot fully capture the complex, nonlinear coupling between solidification microstructure evolution and casting defects. Thus, the optimal parameter set identified by the proposed framework may not ensure uniform quality in mass production. Second, validation remains challenging. The robust parameter calibration for gravity casting demands repeated experiments, which is time-consuming and costly, hindering widespread adoption and scaling from lab optimization to industrial deployment. Overcoming these hurdles are the future topics of this study.

The structure of this paper is as follows. In Sect. 2, we present the bearing seat's dimensions, material, and gravity casting process parameter optimization procedures. In Sect. 3, we describe in detail the experimental design and data collection. In Sect. 4, we provide the statistical analysis of the experimental results. In Sect. 5, we introduce DOA and evaluate the multi-objective optimization, followed by experiments using the optimal parameters. The study concludes with final remarks.

2. Materials and Methods

Figure 1 shows the bearing seat castings and dimensions. Nodular iron QT400-18, whose chemical makeup is listed in Table 1, is selected as the bearing seat material.

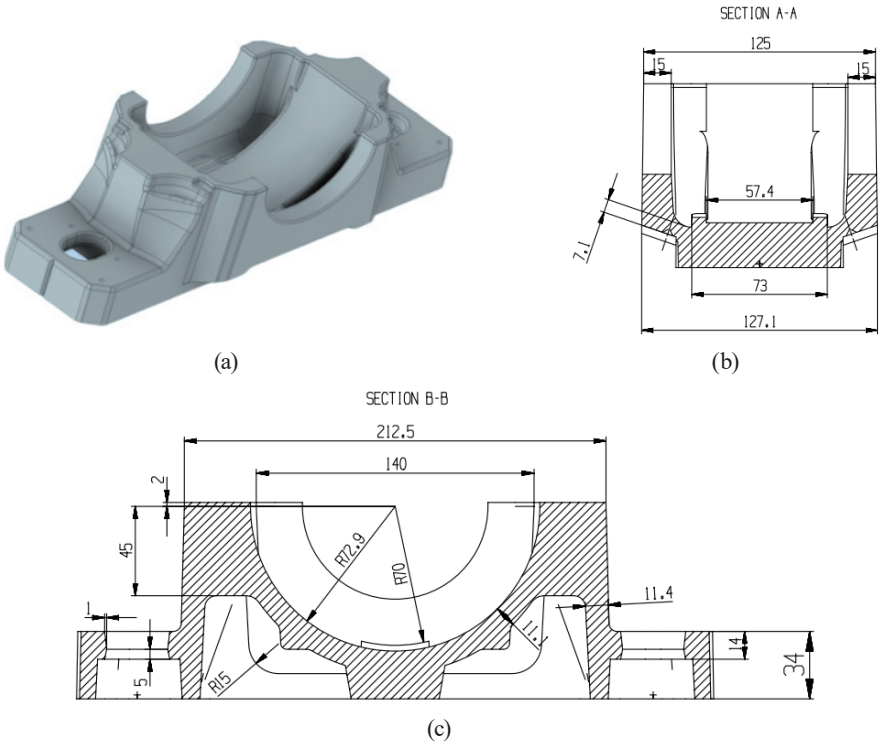

Fig. 1. (Color online) Schematic diagram of bearing seat. (a) Schematic diagram and (b), (c) CAD dimensions.

Table 1
Composition of nodular iron QT400-18.

Element	C	Si	Mn	P	S	Mg	Re
Mass fraction (%)	3.5 to 3.6	2.5 to 3.0	0.45 to 0.57	0.05 to 0.06	0.012 to 0.03	0.03 to 0.06	0.03 to 0.05
Measured value (%)	3.50	3.12	0.14	0.04	0.01	0.04	–

In gravity casting, the production of defect-free components with consistent mechanical properties critically depends on optimal selections of key process variables, including mold and alloy compositions, as well as part geometry. However, traditional experiments only test discrete and predefined parameter sets, making global optimization across the full design space impractical. Empirical selections of a few process parameters are applied in practical gravity casting technologies.

Practitioners thus often rely on heuristic or literature-based parameter estimates, hindering holistic tuning. To address this, hybrid modeling is increasingly adopted, such as a physics-informed or regression-based surrogate. The model, built from historical or targeted experimental data, is coupled with computational optimization to identify high-performance parameter combinations. Consequently, to ensure the structural reliability of casting products, comprehensive defect evaluation technique are essential, such as X-ray radiography and metallography.

Our team has developed a finite element model and numerical simulation software for the gravity casting of bearing seats. This enables us to simulate the casting process while considering how various factors affect the performance of cast components. In this study, using RSM, we empirically select and analyze the impact of three key factors, namely, pouring temperature, mold temperature, and pouring speed, on the quality metrics of bearing seat castings and optimize these parameters. The methods and stages for optimizing gravity casting process parameters are detailed in Fig. 2.

The specific procedures for this task are as follows.

Step 1. Determine the casting process settings for the bearing seat, including pouring temperature, mold temperature, and pouring speed, along with quality metrics such as *DVF* and average *SDAS*.

Step 2. Plan a total of 17 casting experiments using BBD, identifying specific combinations of casting process factors for each experiment. Utilize the previously developed numerical simulation software to compute data related to the 17 quality indicators from these experiments.

Step 3. Create a nonlinear regression model based on Step 2 data, establish the response surface function, and conduct ANOVA to assess its accuracy.

Step 4. Use DAO alongside the response surface function from Step 3 to identify optimal parameter enhancement solutions.

Step 5. Apply optimized parameters from Step 4 in real casting processes to identify key factors for optimization; then, perform gravity casting trials to evaluate if cast component quality meets expected performance standards.

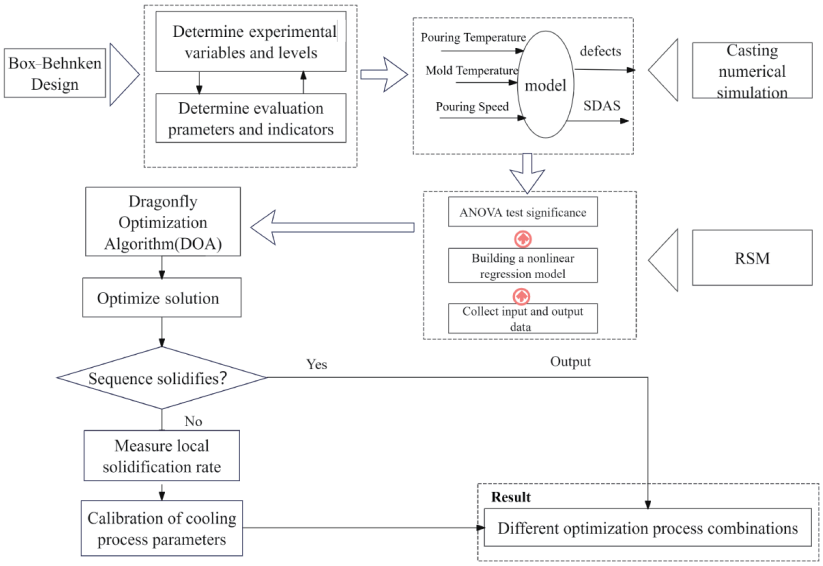

Fig. 2. (Color online) Flowchart for the optimization of gravity casting.

3. Design of Experiments and Collection of Response Data

3.1 Determination of key factors affecting gravity casting

By using the developed gravity casting finite element model and numerical simulation software, we discuss the key factors affecting the casting process. Among other factors, pouring temperature affects gravity casting. A low pouring temperature can lead to cold closes, misruns, and underfilling as the metal liquid hardens before filling is complete. Conversely, a high temperature increases the risk of hydrogen absorption from the atmosphere, leading to H_2-related porosity. It also makes the mold more prone to thermal erosion and cracking, shortening its lifespan. Therefore, on the basis of practical production experience, a control casting temperature range of 1380 to 1420 °C is recommended.

A higher mold temperature slows metal solidification, resulting in a coarser microstructure and increased shrinkage and porosity. Conversely, a lower mold temperature can lead to underfilling due to poor liquid flow. On the basis of current production practices, where mold temperatures are typically managed between 150 and 200 °C in bearing seat manufacturing, we selected a mold temperature range of 150 to 200 °C.

An increase in pouring speed enhances heat transfer between the casting and the mold during solidification, reducing solidification time and increasing structural density. However, excessively high pouring speeds can negatively affect surface quality and dimensional accuracy, while low velocities may induce internal stresses leading to deformation, warping, or cracking. Therefore, it is crucial to set an appropriate pouring speed. In this research, we explored a wide range of pouring speeds for bearing seat castings based on Majidi and Beckermann's concept[26] of locally eliminating bearing seat flaws through gravity casting. The selected range is 0.05 to 0.07 m/s.

This led to the selection of pouring temperature, pouring speed, and mold temperature as test factors, as indicated in Table 2.

3.2 Assessment of quality metrics for cast components

Since shrinkage is the most common defect in the gravity casting of bearing seats, current quality assessments primarily focus on *DVF*. In this study, we applied the Niyama criterion[27] to quantitatively estimate the defect rate of bearing-seat castings. Specifically, we examined how the ratio of temperature gradient to cooling rate changes over time at each node during solidification, aiding in predicting shrinkage defects. The mathematical model presented in Ref. 27 can be described as

$$N_y^* = G/\sqrt{R} < C\,. \tag{1}$$

Here, N_y^* is the value of the criterion function, G is the temperature gradient (°C/m), and R is the cooling rate defined by

$$R = \left|T_u - T_l\right| / \left|t_u - t_l\right|. \tag{2}$$

C is the critical value dependent on casting size, T_u is the liquidus temperature (°C), T_l is the solid phase line temperature (°C), t_u is the liquidus temperature time (s), and t_l is the solid line temperature time (s).

The mechanical characteristics of castings are significantly affected by *SDAS*. Most cracks, as shown in Fig. 3, are concentrated near the stress areas around the bearing holes on the large flat surface. A smaller *SDAS* results in a denser structure and improved mechanical properties. Therefore, reducing *SDAS* is essential. It is clear that if there are no X-ray-grade defects in the casting, the mechanical properties at the bearing seat should be optimized.

According to the Furer–Wunderin model provided in Ref. 28, the width of coarser secondary dendrites increases continuously, whereas smaller secondary dendrites melt more consistently. This model underpins the quantitative relationship developed between local solidification time and *SDAS*. In this study, *SDAS* is calculated using the Furer–Wunderin model.[28]

$$\lambda = 5.5(\mathrm{A}t_f)^{1/3} \tag{3}$$

Here, λ is the secondary dendrite spacing, t_f is the solidification time of a certain spatial position (s), and A is the coarsening coefficient evaluated as

Table 2
Experimental variables and levels.

Process parameters	ID	Level 1	Level 2	Level 3
Pouring temperature (°C)	X_1	1380	1400	1420
Mold temperature (°C)	X_2	100	125	150
Pouring speed (m/s)	X_3	0.05	0.06	0.07

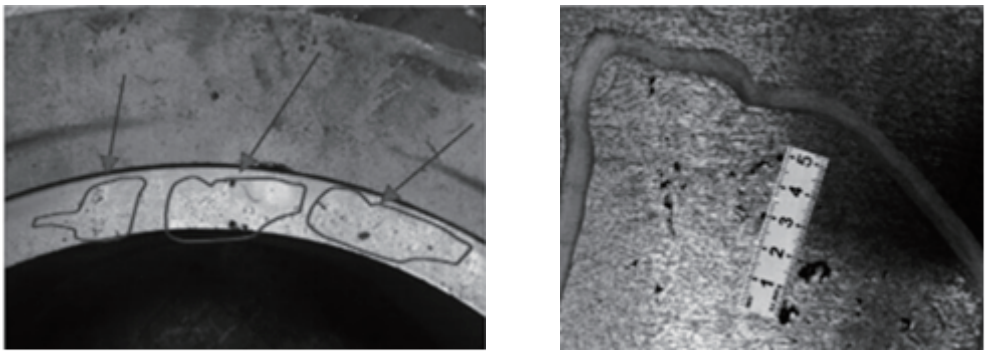

(a) (b)

Fig. 3. Crack location maps. (a) Bearing seat crack and (b) crack development diagram.

$$A = \tau D_L \ln(C_0/C_L)/\left[m_L(1-k)(C_0 - C_L)\right], \tag{4}$$

where τ is the Gibbs–Thompson coefficient, D_L is the solute diffusion coefficient in the liquid phase, C_L is the liquid phase concentration (mol/L), C_0 is the original concentration of the alloy liquid (mol/L), m_L is the liquidus slope, and k is the equilibrium distribution coefficient.

The formula above shows the proportional relationship between *SDAS* and local solidification time. Specifically, *SDAS* increases with longer local solidification times or lower solidification rates.

3.3 Design of gravity casting experiments

One experimental design technique for assessing nonlinear relationships between parameters and performance indicators is BBD. After determining the testing criteria and amounts, BBD was applied. Unlike central repeat tests, BBD does not require consecutive testing, resulting in fewer test combinations under the same conditions, making it more cost-effective.[29]

The experiments in this study were generated using Design-Expert 13 software. A total of seventeen experiment groups were produced according to BBD, as shown in Table 3. The gathered reaction data were entered into the software for the assessment of the BBD experimental results, which are then thoroughly analyzed.

3.4 Collection of response data

In accordance with BBD for casting experiments, the *DVF* and average *SDAS* of the bearing seat's bear holes are obtained by simulating the gravity casting process 17 times using simulation software, as shown in Table 3. Retaining extra significant digits, even if unmeasurable, is crucial for enhancing the accuracy of the subsequent mathematical model owing to unclear simulation results. The predictive power of this model relies on its accuracy.

Table 3
Designed experiments and corresponding response data.

Exp. No.	Process parameters			Response data	
	X_1	X_2	X_3	Y_1 : *DVF* (%)	Y_2 : *SDAS* (μm)
1	1400	150	0.05	0.574	37.43
2	1380	125	0.05	0.426	25.96
3	1400	125	0.06	0.55	36.14
4	1400	150	0.07	0.457	38.03
5	1380	125	0.07	0.372	25.22
6	1420	125	0.07	0.663	43.00
7	1400	100	0.07	0.424	32.08
8	1400	125	0.06	0.543	37.77
9	1400	150	0.06	0.517	36.52
10	1420	100	0.06	0.596	38.35
11	1400	125	0.05	0.577	36.23
12	1420	125	0.05	0.678	40.08
13	1380	150	0.06	0.461	28.80
14	1420	150	0.06	0.727	42.99
15	1380	100	0.06	0.411	26.35
16	1400	100	0.05	0.424	32.94
17	1420	125	0.06	0.565	38.11

4. Statistical Analysis and Optimization

4.1 Building a nonlinear regression model

The nonlinear input–output mapping model, or response surface for casting process parameters, is established using simulation output data such as *DVF* and average *SDAS* of the bearing holes in the bearing seat. ANOVA assesses the model's relevance and predictive power after regression analysis.[30] Two nonlinear *DVF* and *SDAS* input–output mapping models are developed.

In this study, we propose a more accurate method to combine process parameters by utilizing DOA to optimize them, achieving an approximated globally optimal solution based on multi-objective outcomes with the developed mapping model. The suitable combination of process parameters is validated in actual production through thorough optimization. The main methods for verifying the improved process solution's feasibility include the inspection of bearing seat quality and the testing of related mechanical properties.

4.2 Results and discussion

4.2.1 *DVF* analysis

DVF as a response indicator and the regression model is evaluated as

$$\begin{aligned} Y_1 = {} & 0.5504 + 0.1243X_1 + 0.0455X_2 - 0.0232X_3 + 0.02022X_1X_2 \\ & + 0.0098X_1X_3 - 0.0292X_2X_3 + 0.0317X_1^2 - 0.0333X_2^2 - 0.0473X_3^2. \end{aligned} \tag{5}$$

As indicated in Tables 4 and 5, the fitted model is acquired, and ANOVA is used to evaluate the model's suitability. The model can predict the direction of the test factors' effect on the response index, as evidenced by its exceptional significance (p-value < 0.0001) and lack of significance (misfit).

In Table 5, R^2 increases with the number of variables added, but a correct model should have several coefficients of determination, which are larger than 0.9 and closer to 1. The modified adjusted R^2 is therefore commonly used to express the correlation. The model's high reliability is demonstrated by the coefficient of variation (CV) being less than 10%, which falls within a reasonable range, and by the fact that the R^2 and adjusted R^2 in this model are more significant than 0.9.[31]

Figure 4(a) shows the normal probability plot of the model residuals that follow a straight line and obey a normal distribution. Figure 4(b) shows the linear line distribution of the expected response and actual values.

4.2.2 *SDAS* analysis

The average *SDAS* as a response indicator and the regression model is determined as

$$Y_2 = 36.95 + 7.26X_1 + 2.19X_2 + 0.2400X_3 + 0.5475X_1X_2 + 0.9150X_1X_3 + 0.3650X_2X_3 - 2.19X_1^2 - 0.6383X_2^2 + 1.20X_3^2. \quad (6)$$

Table 4
DVF response model analysis of variance.

Source	Sum of squares	*df*	Mean Square	*F*-value	*p*-value	
Model	0.1678	9	0.0186	37.97	< 0.0001	significant
X_1	0.1235	1	0.1235	251.49	< 0.0001	
X_2	0.0166	1	0.0166	33.72	0.0007	
X_3	0.0043	1	0.0043	8.81	0.0209	
X_1X_2	0.0016	1	0.0016	3.34	0.1103	
X_1X_3	0.0004	1	0.0004	0.7743	0.4081	
X_2X_3	0.0034	1	0.0034	6.97	0.0334	
X_1^2	0.0042	1	0.0042	8.60	0.0219	
X_2^2	0.0047	1	0.0047	9.52	0.0177	
X_3^2	0.0094	1	0.0094	19.20	0.0032	
Residual	0.0034	7	0.0005			
Lack of fit	0.0013	3	0.0004	0.8585	0.5312	not significant
Pure error	0.0021	4	0.0005			
Cor total	0.1712	16				

Table 5
Summary of *DVF* model fitting results.

Std. dev.	Mean	*C.V.* %	R^2	Adjusted R^2	Predicted R^2	Adeq precision
0.0222	0.5274	4.20	0.9799	0.9541	0.8551	21.2543

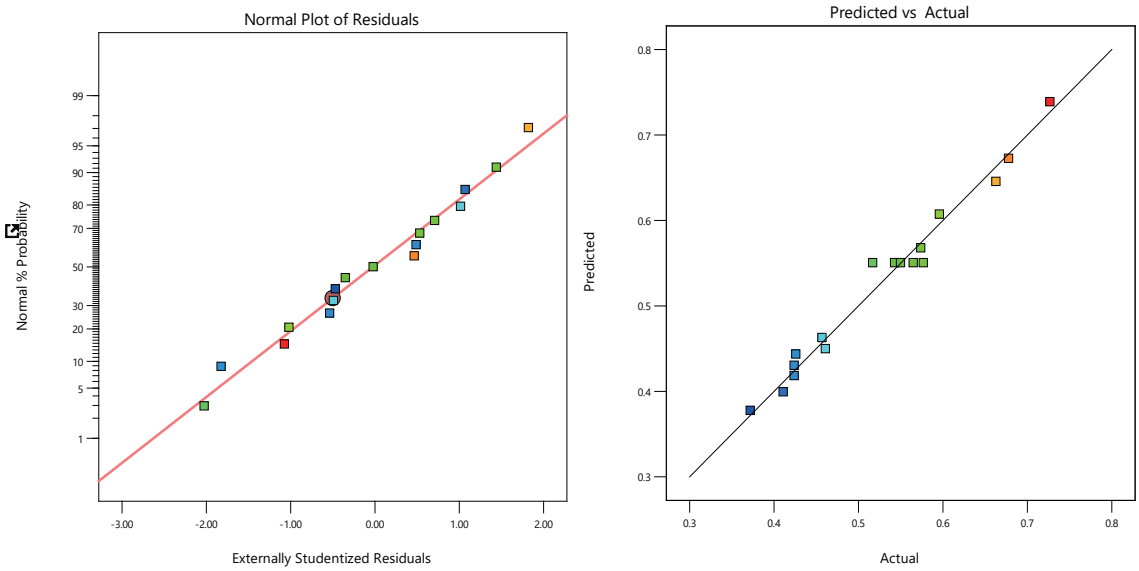

(a) (b)

Fig. 4. (Color online) Response diagnostic chart. (a) Residual normal probability and (b) predicted and actual distributions.

The average *SDAS* response model by ANOVA is shown in Tables 6 and 7. The predictive power of the model is strong, as indicated by the p-value < 0.0001 and the insignificance of the out-of-fit term. The model is deemed reliable with a CV of 3.34% and R^2 and adjusted R^2 values near 1.

The normal probability plot of the model residuals, which shows normal and linear distributions, is shown in Fig. 5(a). The expected and actual response values are shown in Fig. 5(b), where they both follow a linear distribution. The response surface study demonstrates that pouring temperature is a critical component of *SDAS*. It has a substantially higher effect rate than pouring speed and mold temperature in this selection range. By reducing the mold temperature and carefully choosing the pouring speed, *SDAS* can be reduced to improve the mechanical properties of the bearing seat.

5. Multi-objective Optimization by DOA

5.1 DOA

In 2016, Mirjalili introduced DOA,[25] a swarm-based optimization method inspired by dragonflies' survival-related social interactions.[32,33] The group dynamics of dragonflies can be categorized into five phases:[33,34] (1) Separation, where they avoid collisions with stationary objects; (2) Alignment, in which individuals match their flight velocities to others; (3) Cohesion, reflecting the tendency to gather near the group's center; (4) Attraction to food sources, capturing individual responses upon locating food; and (5) Distraction of predators, addressing potential threats to the group. DOA utilizes both dynamic and static behaviors observed in dragonflies as

Table 6
Average *SDAS* response model by ANOVA.

Source	Sum of squares	*df*	Mean square	*F*-value	*p*-value	
Model	496.17	9	55.13	40.20	< 0.0001	significant
X_1	421.81	1	421.81	307.57	< 0.0001	
X_2	38.41	1	38.41	28.01	0.0011	
X_3	0.4608	1	0.4608	0.3360	0.5803	
X_1X_2	1.20	1	1.20	0.8743	0.3809	
X_1X_3	3.35	1	3.35	2.44	0.1621	
X_2X_3	0.5329	1	0.5329	0.3886	0.5528	
X_1^2	20.25	1	20.25	14.77	0.0063	
X_2^2	1.72	1	1.72	1.25	0.3003	
X_3^2	6.02	1	6.02	4.39	0.0744	
Residual	9.60	7	1.37			
Lack of Fit	6.22	3	2.07	2.46	0.2027	not significant
Pure Error	3.38	4	0.8443			
Cor Total	505.77	16				

Table 7
Secondary dendrite spacing model fitting results.

Std. ev.	Mean	*C.V.* %	R^2	Adjusted R^2	Predicted R^2	Adeq precision
1.17	35.06	3.34	0.9810	0.9566	0.7927	21.0483

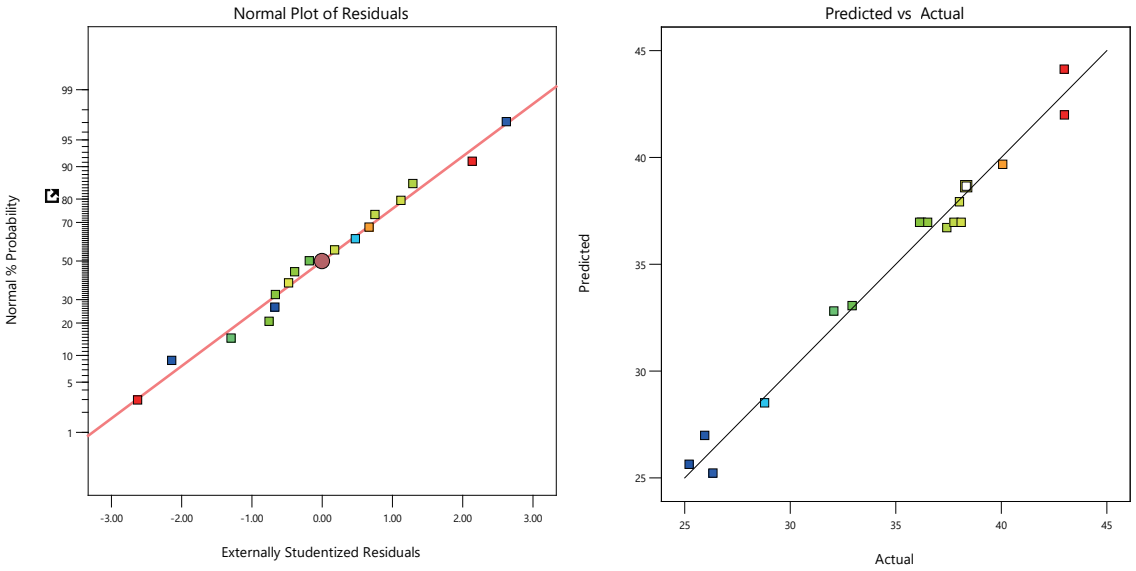

Fig. 5. Response diagnostic chart. (a) Residual normal probability and (b) predicted and actual distribution.

an optimization framework for data processing. In this study, we provide a concise overview of the two data processing stages enabled by DOA.[32,35]

Stage 1: Exploration Phase. In the initial exploration phase, dragonflies form small clusters and travel short distances to find food sources and attract flying prey. The main goal is to

expand the search area to identify potential food-rich zones or ideal solutions. Subsequently, the cluster will explore additional areas using targeted approaches.

Stage 2: Exploitation Phase. During this stage, an increase in dragonfly population leads to a coordinated movement toward a specific direction, diverting attention from enemies. The primary objective is to analyze and refine the data collected during the exploration phase, focusing on improving the most promising solutions identified earlier.

DOA comprises five distinct operation types based on exploration and development stages.

(1) Separation operation (SO):

This process aims to prevent potential collisions among artificial dragonflies in the swarm, calculated as

$$SO(\alpha,\gamma) = -\sum_{\beta=1}^{N} (Z(\alpha,\gamma) - Z(\beta,\gamma)) . \tag{7}$$

Here, $SO(\alpha, \gamma)$ is the SO between they α-th solution and the neighboring γ-th iteration. $Z(\alpha, \gamma)$ is the situation of the α-th solution in the γ-th iteration. $Z(\beta, \gamma)$ is the situation of the β-th solution in the γ-th iteration. N is the number of neighboring solutions.

(2) Alignment operation (AO):

This operation regulates the flight speed of artificial dragonflies in the swarm to maintain optimal distances for successful colonization. The formula for computing AO is

$$AO(\alpha,\gamma) = \frac{1}{N}\sum_{\beta=1}^{N} V(\alpha,\gamma) . \tag{8}$$

Here, $AO(\alpha, \gamma)$ is the AO for the α-th solution in the γ-th iteration. $V(\alpha, \gamma)$ is the velocity for the β-th neighboring solution in the γ-th iteration.

(3) Cohesion operation (CO):

This operation aims to maintain the cohesive integrity of the dragonfly group by guiding all artificial dragonflies toward the group's centroid using a systematic strategy. The computation of CO involves Eq. (9).

$$CO(\alpha,\gamma) = \frac{1}{N}\sum_{\beta=1}^{N} Z(\beta,\gamma) - Z(\alpha,\gamma) \tag{9}$$

Here, $CO(\alpha, \gamma)$ is the CO for the α-th solution in the γ-th iteration.

(4) Food attraction operation (FAO):

This operation guides artificial dragonflies to food sources. The level of food attraction can be measured as

$$FA(\alpha,\gamma) = Z^{+} - Z(\alpha,\gamma) . \tag{10}$$

Here, $FA(\alpha, \gamma)$ is the food attraction for the α-th solution in the γ-th iteration. Z^+ is the situation of the food in the γ-th iteration.

(5) Enemy distraction operation (EDO):

This operation involves generating a deceptive signal to mislead the enemy, redirecting them away from the dragonfly group's intended destination. The following formula can be used to measure the effectiveness of this distraction.

$$ED(\alpha,\gamma) = Z^- + Z(\alpha,\gamma) \tag{11}$$

$ED(\alpha, \gamma)$ is the EDO for the α-th solution in the γ-th iteration. Z^- is the location of the enemy in the γ-th iteration.

The adaptive integration of prior operational data allows for precise adjustments to the artificial dragonfly's location. Each cycle refines the position by combining the movement vector $\Delta Z(\alpha, \gamma)$ and the positional vector $Z(\alpha, \gamma)$. The movement vectors used to control the locations of artificial dragonflies within the DOA framework are mathematically defined by

$$\begin{aligned}\Delta Z(\alpha,\gamma+1) = {} & \rho_S SO(\alpha,\gamma) + \rho_A AO(\alpha,\gamma) + \rho_C CO(\alpha,\gamma) \\ & + \rho_F FA(\alpha,\gamma) + \rho_E ED(\alpha,\gamma) + \mu\Delta Z(\alpha,\gamma),\end{aligned} \tag{12}$$

where ρ_S, ρ_A, ρ_C, ρ_F, and ρ_E are the weights of the operations of separation, alignment, cohesion, food attraction, and enemy distraction, respectively. μ is the weight of inertia. The updated position of the artificial dragonfly can be calculated as

$$Z(\alpha,\gamma+1) = Z(\alpha,\gamma) + \Delta Z(\alpha,\gamma). \tag{13}$$

By summarizing the aforementioned steps, the flowchart illustrating the evaluation process of DOA is presented in Fig. 6.

5.2 Evaluation of DOA for multi-objective optimization

Using the previously mentioned experimental and simulation data, we developed a response surface function for bearing seat gravity casting, specifically as a nonlinear input–output regression model. Subsequently, the quality and performance of cast components are improved through experimental design techniques. This enhancement involved selecting optimal casting parameters, namely, pouring temperature, mold temperature, and pouring speed, to reduce both the *DVF* and average *SDAS* of the cast components. A composite objective function was created by assigning appropriate weight factors to *DVF* and normalized average *SDAS* values. Equation (14) is the mathematical representation of this composite objective function.

$$Z(X_1, X_2, X_3) = \omega_1 Y_1 + \omega_2 \overline{Y}_2 \tag{14}$$

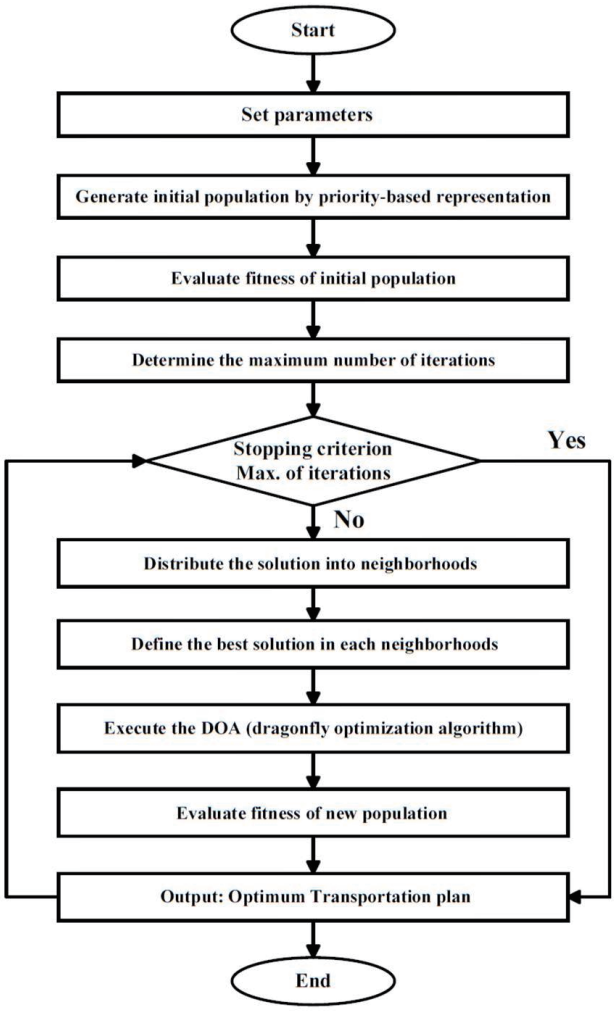

Fig. 6. Flowchart of DOA.

In this context, X_1, X_2, and X_3 correspond to pouring temperature, mold temperature, and pouring speed, respectively. Additionally, $\bar{Y}_1$ and $\bar{Y}_2$ refer to *DVF* and the normalized average *SDAS*, respectively. Within this research, $\overline{Y_2} = (Y_2 - 10)/40$ is determined by considering the typical range of the average *SDAS*, which falls between 10 and 50 μm, as supported by prior experimental data. The terms ω_1 and ω_2 serve as weighting coefficients that adhere to the condition $\omega_1 + \omega_2 = 1$. As a result, the optimization challenge is structured as outlined below.

$$\begin{aligned} &\text{Minimize } Z(X_1, X_2, X_3), \text{subject to} \\ &1380\ ^\circ\text{C} \le X_1 \le 1420\ ^\circ\text{C}, 100\ ^\circ\text{C} \le X_2 \le 150\ ^\circ\text{C}, 0.05\ \text{m/s} \le X_3 \le 0.07\ \text{m/s} \end{aligned} \tag{15}$$

To evaluate and compare the outcomes of DOA, we employed the Archimedes optimization algorithm (AOA)[36] to tackle the optimization challenge in Eq. (15). Simulations are conducted on a system with Microsoft Windows 11 (64-bit), a Core i7 processor at 2.5 GHz, and 16 GB of

RAM. A population size of 80 is set, with each optimization algorithm undergoing 40 iterations during the process. The weighting factors are denoted as $\omega_1 = 0.75$ and $\omega_2 = 0.25$.

The convergence curves for AOA and DOA are shown in Fig. 7. DOA achieves a higher optimal value than AOA, requiring only 10 and 25 iterations to reach the optimal functional value, respectively. This indicates that DOA converges to the optimal solution with fewer iterations. To demonstrate the effectiveness of these optimization techniques, Table 8 presents the multi-objective optimization results along with the corresponding gravity casting process parameters.

Once the optimal process parameters were selected, experiments were conducted to verify the associated *DVF* and average *SDAS* under the highest input values identified using DOA. Table 9 presents the error percentage between the predicted and experimental results. This investigation shows a small estimated error, indicating that the experimental conditions are highly reproducible.

Furthermore, the real bearing seat casting was performed using gravity casting parameters obtained through DOA. The 100× metallographic image is shown in Fig. 8. Defect locations in

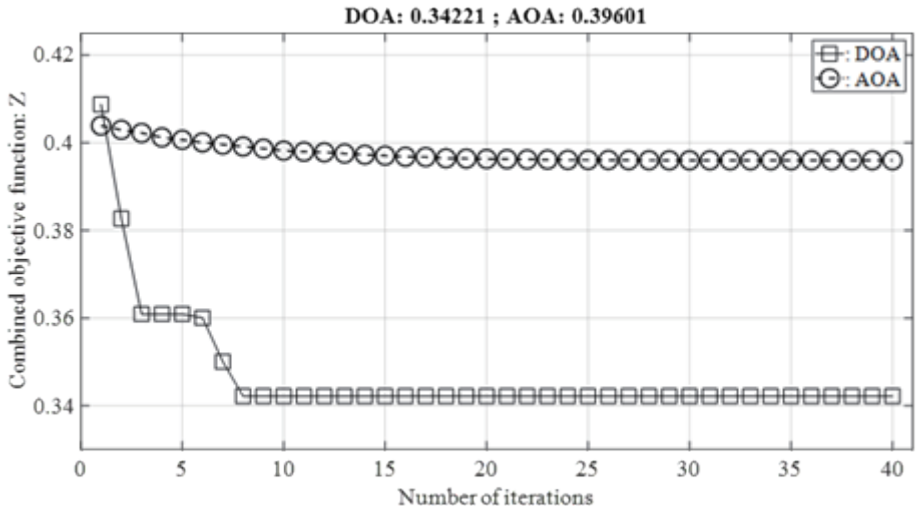

Fig. 7. Convergent curves of DOA and AOA.

Table 8
Multi-objective optimization results of DOA and AOA.

Algorithm	Z	X_1	X_2	X_3
DOA	0.34221	1380	100	0.07
AOA	0.39601	1380	124	0.0686

Table 9
Multi-objective optimization results of DOA.

	DVF (%)	*SDAS* (μm)
Prediction by DOA	0.3481	22.9792
Experiment	0.3562	23.1944
Error (%)	2.3269	0.9583

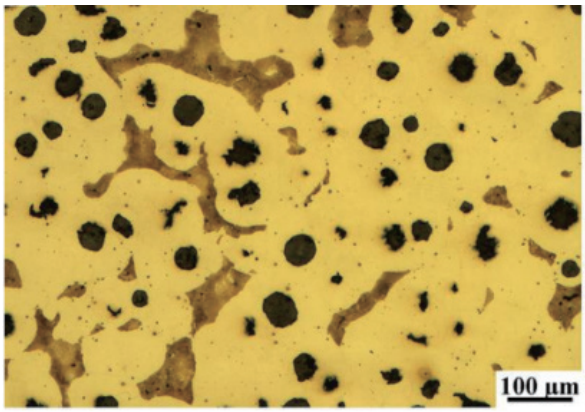

Fig. 8. (Color online) Metallographic image at 100× magnification.

the cast components are approximately 7 μm from the inner wall of the casting, closely aligning with final solidification areas. This confirms that the simulation results of solid-liquid distribution can accurately predict defect locations, providing a basis for process optimization.

6. Conclusions

In this study, we proposed a multi-objective optimization framework, which is the combined casting process simulation, RSM, DOA, and quality detection of casting product by X-ray detection, to optimize gravity casting parameters for wind turbine bearing seats. Using BBD, three key factors were selected, leading to the development of a validated nonlinear model via ANOVA. The optimized casting process parameters were confirmed through experimental validation. Results showed minimal estimation errors, ensuring consistency in the experimental setup. However, the proposed approach has limitations, including uneven casting quality from oversimplified model optimization, and costly, time-consuming experimental validation. Our future work will focus on overcoming these pending problems.

Acknowledgments

This work was supported in part by the Open Project Program of Fujian Key Laboratory of Special Intelligent Equipment Measurement and Control, Fujian Special Equipment Inspection and Research Institute (Grant No. FJIES2024KF17), the Teaching Reform Research Project of Sanming University (Grant No. J202426), the Higher Education Research Project of Sanming University (Grant No. SHE2413), the Operational Funding of the Advanced Talents for Scientific Research (Grant No. 19YG04) of Sanming University, the Natural Science Foundation of Sanming University (Grant No. KD23003P), and the Program for Innovative Research Team in Science and Technology in Fujian Province University. The authors also acknowledge the support from the School of Mechanical and Electric Engineering, Sanming University.

References

1 T. M. Letcher: Wind Energy Engineering: A Handbook for onshore and offshore wind turbines (Elsevier, London, UK, 2017) p. 145.
2 O. Shamet, M. Sofian, S. M. Alawad, M. Asif, and M. Antar: Arab. J. Sci. Eng. online published: 06 April 2025. https://doi.org/10.1007/s13369-025-10159-0
3 I. Gohar, W. K. Yew, A. Halimi, and J. See: Eng. Appl. Artif. Intell. **14** (2025) 109970. https://doi.org/10.1016/j.engappai.2024.109970
4 J. Asensio-Lozano, J. F. Alvatz-Antolín, and C. H. Alvarez-Pérez: Revista de Metalurgia **54** (2018) e118. https://doi.org/10.3989/revmetalm.118
5 J. Campbell: Complete casting handbook: Metal casting processes, techniques and design (2nd ed.) (Elsevier, Waltham US, 2015) p. 529.
6 S. Khan Afridi, M. A. Koondhar, M. I. Jamali, Z. Alaas, M. H. Alsharif, M. K. Kim, I. Mahariq, E. Touti, M. Aoudia, and M. Ahmed: IEEE Access **12** (2024) 66147. https://doi.org/10.1109/ACCESS.2024.3397243
7 Z. Liao, I. Sanchez, D. Xu, D. Axinte, G. Augustinavicius, and A. Wretland: J. Mater. Process. Technol. **285** (2020) 116768. https://doi.org/10.1016/j.jmatprotec.2020.116768
8 A. J. Santhosh and A. R. Lakshmanan: China Foundry **13** (2016) 352. https://doi.org/10.1007/s41230-016-5078-y
9 A. Karthik, R. Karunanithi, S. A. Srinivasan, and M. Prashanth: Mater. Today Proc. **27** (2020) 2556. https://doi.org/10.1016/j.matpr.2019.10.136
10 F. Inegbediona, E. U. Ikponmwenb, and D. U. Ezuma: Adv. Eng. Des. Technol. **4** (2022) 54. https://doi.org/10.37933/nipes.a/4.1.2022.6
11 B. Jiang, J. Huang, H. Ma, H. Zhao, and H. Ji: Materials **15** (2022) 8350. https://doi.org/10.3390/ma15238350
12 M. R. Shivakumar and M. K. Panchangam: Heliyon **10** (2024) e30183. https://doi.org/10.1016/j.heliyon.2024.e30183
13 L. Zhang, L. Li, S. Wang, and B. Zhu: J. Mater. Eng. Perform. **21** (2011) 492. https://doi.org/10.1007/s11665-011-9933-0
14 A. K. Gupta, S. Kumar, P. Chandna, and G. Bhushan: Silicon **13** (2021) 2429. https://doi.org/10.1007/s12633-020-00594-z
15 J. Deng, B. Xie, D. You, L. Wang, X. Wu, G. Liu, and J. Liang: J. Manuf. Processes **84** (2022) 1320. https://doi.org/10.1016/j.jmapro.2022.10.074
16 J. Li, Y. Sun, Y. Wang, and J. Sun: Int. J. Adv. Manuf. Technol. **118** (2022) 3421. https://doi.org/10.1007/s00170-021-08099-8
17 M. W. Fu and M. S. Yong: Int. J. Prod. Res. **47** (2009) 5203. https://doi.org/10.1080/00207540801935616
18 J. Zeng, G. Li, Z. Gao, Y. Li, S. Sundararajan, S. Barbat, and Z. Hu: Struct. Multidisc. Optim. **66** (2023) 96. https://doi.org/10.1007/s00158-023-03553-5
19 K. Dou, E. Lordan, Y. J. Zhang, A. Jacot, and Z. Y. Fan: J. Manuf. Processes **60** (2020) 435. https://doi.org/10.1016/j.jmapro.2020.10.062
20 E. Chen, H. Li, H. Cao, and X. Wen: Front. Mech. Eng. **16** (2021) 868. https://doi.org/10.1007/s11465-021-0656-0
21 C. P. Kohar, L. Greve, T. K. Eller, D. S. Connolly, and K. Inal: Comput. Methods Appl. Mech. Eng. **385** (2021) 114008. https://doi.org/10.1016/j.cma.2021.114008
22 K. Dou, E. Lordan, Y. J. Zhang, A. Jacot, and Z. Y. Fan: J. Manuf. Processes **60** (2020) 435. https://doi.org/10.1016/j.jmapro.2020.10.062
23 Q. Zheng, Y. Xiao, T. Zhang, P. Zhu, W. Ma, and J. Liu: Metals **10** (2020) 1024. https://doi.org/10.3390/met10081024
24 Y. He, D. Lu, Z. Li, and D. Lu: Materials **16** (2023) 6223. https://doi.org/10.3390/ma16186223
25 S. Mirjalili: Neural Comput. Appl. **27** (2016) 1053. https://doi.org/10.1007/s00521-015-1920-1
26 S. H. Majidi and C. Beckermann: Int. J. Cast Met. Res. **30** (2017) 301. https://doi.org/10.1080/13640461.2017.1307624
27 K. D. Carlson and C. Beckermann: Metall. Mater. Trans. A **40** (2009) 163. https://doi.org/10.1007/s11661-008-9715-y
28 W. Kurz, D. J. Fisher, and M. Rappaz: Fundamentals of solidification (Trans. Tech. Publications Ltd., Baech, Switzerland, 2023) 5th ed., p. 173.
29 A. Tamilarasan and A. Renugambal: Mater. Manuf. Processes **38** (2023) 1130. https://doi.org/10.1080/10426914.2023.2165673
30 G. Singh and P. K. Singh: Mater. Manuf. Processes **38** (2022) 206. https://doi.org/10.1080/10426914.2022.2075894

31 C. Manikandan, K. S. Amirthagadeswaran, and N. Gunasekaran: Mater. Res. Express **8** (2021) 076512. https://doi.org/10.1088/2053-1591/ac10d4
32 C. M. Rahman, T. A. Rashid, A. Alsadoon, N. Bacanin, P. Fattah, and S. Mirjalili: Evol. Intell. **16** (2023) 1. https://doi.org/10.1007/s12065-021-00659-x
33 Y. Meraihi, A. Ramdane-Cherif, D. Acheli, and M. Mahseur: Neural Comput. Appl. **32** (2020) 16625. https://doi.org/10.1007/s00521-020-04866-y
34 D. Hendardi, W. F. Josephen, H. L. H. S. Warnars, E. Abdurrachman, P. Assiroj, A. I. Kistijantoro, and A. Doucet: Commun. Math. Biol. Neurosci. **47** (2021) 1. https://doi.org/10.28919/cmbn/5767
35 M. Alshinwan, L. Abualigah, M. Shehab, M. A. Elaziz, A. M. Khasawneh, H. Alabool, and H. A. Hamad: Multimedia Tools Appl. **80** (2021) 14979. https://doi.org/10.1007/s11042-020-10255-3
36 F. A. Hashim, K. Hussain, E. H. Houssein, M. S. Mabrouk, and W. Al-Atabany: Appl. Intell. **51** (2021) 1531. https://doi.org/10.1007/s10489-020-01893-z